PIER Letters

(Received 11 June 2024, Accepted 18 July 2024, Scheduled 18 August 2024)

A Compact Low-Loss Single-Layer Vialess Diplexer Based on Complementary Microstrip Spiral Resonators for Satellite Communications

Giacomo Giannetti*, Stefano Maddio, and Stefano Selleri

Department of Information Engineering, University of Florence, Florence, I-50137, Italy

ABSTRACT: The design of a compact low-loss diplexer based on complementary microstrip spiral resonators is described. The resonant elements are two: one is low-pass (channel A) and the other is passband (channel B). The low-pass element is composed of spirals departing from a circle, whereas the passband element is composed of spirals etched on a circle. The former element is novel and has been extensively analyzed here. These elements are connected using a star nonresonant Y-junction to form a single-layer vialess diplexer. As an example, a diplexer working at 0.87 and 2.0 GHz for satellite communications is manufactured and tested. The measured data show an insertion loss equal to 0.58 dB (0.66 dB) for channel A (B). The return loss exceeds 15 dB for both channels, and the dimensions are $0.129\,\lambda \times 0.265\,\lambda \approx 0.0343\,\lambda^2$.

1. INTRODUCTION

Diplexers are key components in microwave systems, such as radio frequency (RF) front-ends [1, 2], enabling the separation of channels at different frequencies and routing them to separate output ports. However, system miniaturization is always at a premium, due to the coexistence of different subsystems on the same board, hence the smallest possible dimensions for every component, diplexer included, are required. An array of conventional bandpass filters based on coupled resonators [3–5] occupies a large amount of space on the PCB board. Hence, a compact low-loss diplexer based on complementary spiral resonators is proposed here, and the use of passband spiral resonators in microwave filters was initially introduced in [6] and pursued further in [7]. The key point is that, due to the peculiarities of the design, a single resonator suffices to achieve good channel isolation, as shown in the following.

The realization technology is microstrip, and the design is single-layer vialess, making it easy to implement and integrate. The authors have proven the validity of this approach in [8], where a diplexer working at 1.9 GHz and 3.5 GHz has been designed and manufactured. The layout comprises a low-pass spiral resonator, selecting the lower band, and a passband spiral resonator, selecting the higher band. Although this general layout is similar to [8], the design of the low-pass element presented here is substantially different. This novel low-pass element is here considered and analyzed thoroughly.

Spiral resonators are not new. Other than in filters [9] and diplexers [10–12], spiral resonators are used in radio frequency integrated circuit (RFIC) tags [13, 14], wireless power transfer [15], sensors [16, 17], metamaterials [18, 19], and microwave oscillators [20]. These applications are based on either rectangular or circular spiral resonators with a single spiral. On the contrary, resonators with two wrapping spirals are introduced in [8] for the first time and analyzed more in-depth here.

The article is organized as follows. Firstly, the design of the diplexer is outlined, focusing on the analysis of the novel low-pass element. Then, the design of a prototype, as well as its characterization, is presented, focusing on the two bandwidths centered at 0.87 and 2.0 GHz for satellite communications in Europe [21]. The measured and simulated responses are compared, and the performance is evaluated against the existing literature. Eventually, conclusions are drawn.

2. DESIGN

The top layer of the diplexer is depicted in Fig. 1. The common port is P1, while P2 (P3) is the port of channel A (B). The required filtering behaviour is realized by the spiral elements

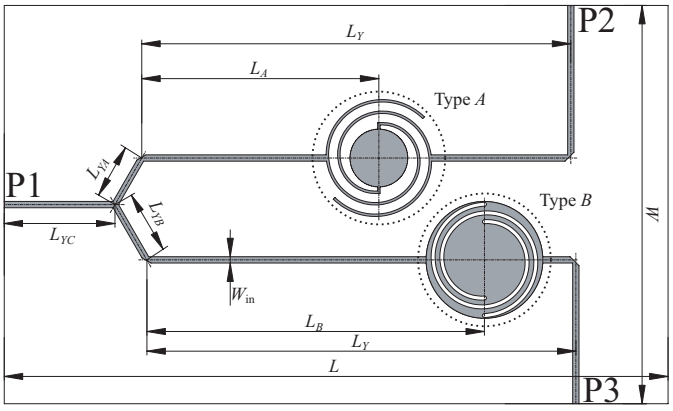

FIGURE 1. Technical drawing of the diplexer.

* Corresponding author: Giacomo Giannetti (giacomo.giannetti@unifi.it).

highlighted by the dotted circles. Throughout the paper, they are called type A and type B. The former is low-pass, while the latter is passband. The two elements are described in the following two subsections. Their filtering behavior is explained by sub-wavelength phenomena [22, 23].

2.1. Type A Element

Type A element presents spirals departing from an inner structure, and its technical drawing is shown in Fig. 2(a). The inner structure comprises a circle of radius R_A and two rectangular radial extensions of width W_A, from which the spirals start. The width of the spirals is also W_A, and the spacing between the turns of different spirals, computed on the midlines, is S_A. The expression of the spiral midline in polar coordinates (ρ, ϕ) is given by

$$\rho(\theta) = (R_e - W_A/2)(1 - \alpha_A\theta) \quad \theta \in [-\theta_A, 0] \qquad (1)$$

with $\alpha_A = S_A/[\pi(R_e - W_A/2)]$ and $G_A = S_A - W_A$. Note that the type A element is fully characterized by five parameters: R_A, W_A, G_A, θ_A, and R_e.

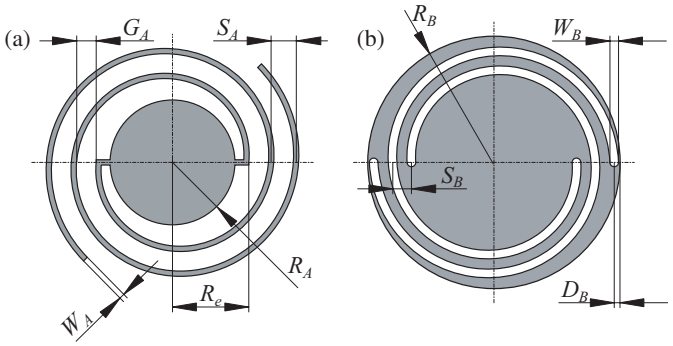

FIGURE 2. Spiral elements: (a) type A; (b) type B.

Since the type A element presented in this paper is an upgrade of the one in [8], with additional degrees of freedom, a detailed analysis is performed here, based on parametric sweeps.

Here and throughout the paper, the substrate is Taconic Cermet10(TM). Its characteristics are: dielectric thickness 0.64 mm, copper thickness 0.018 mm, dielectric relative permittivity 10, and loss tangent 0.0017. In the analysis, the type A element is fed by two straight microstrip lines (Fig. 3) having width $W_{\text{in}} = 0.57$ mm, which corresponds to a characteristic impedance of 50 Ω (computed using the formulae for thick microstrip reported in [24]). The nominal configuration for the parameters is $R_A = 2.6$ mm, $W_A = 0.225$ mm, $G_A = 0.475$ mm, $\theta_A = 410°$, and $R_e = 2.95$ mm. In Fig. 4, the magnitude of the transmission and reflection coefficients in the frequency range 0.1–2.5 GHz is shown as a function of the geometric parameters. From the nominal values, the following sweeps are performed:

- $R_A \in [2.2, 2.4, 2.6, 2.8, 3.0]$ mm in Fig. 4(a);
- $W_A \in [0.175, 0.2, 0.225, 0.25, 0.275]$ mm in Fig. 4(b);
- $G_A \in [0.425, 0.45, 0.475, 0.5, 0.525]$ mm in Fig. 4(c);
- $\theta_A \in [390°, 400°, 410°, 420°, 430°]$ in Fig. 4(d);

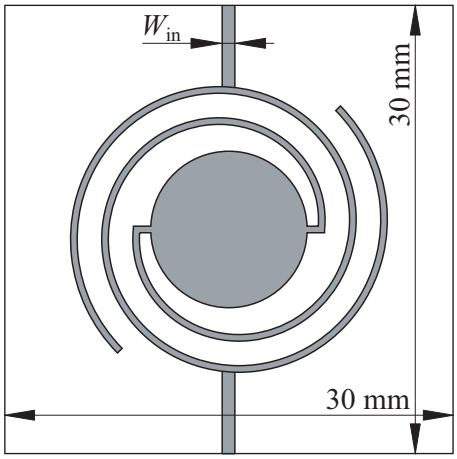

FIGURE 3. Setting for the parametric analysis of type A element. The drawing is not in scale and the substrate edges are at least 10.45 mm away from the spirals to avoid interactions with the resonator.

- $R_e \in [2.75, 2.85, 2.95, 3.05, 3.15]$ mm in Fig. 4(e).

The results in Fig. 4 are obtained using the full-wave simulator CST [25], since the complex shape of the resonator prevents the use of faster semi-analytical methods, such as [26, 27]. From Fig. 4, we note that the type A element presents a low-pass behavior, and the value of R_A has the greatest impact on the cutoff frequency. As a heuristic design rule, the value of R_A returning a given −3 dB-cutoff frequency f_c is

$$R_A\,[\text{mm}] = 6.62 - 4.04 f_c\,[\text{GHz}] + 0.779(f_c\,[\text{GHz}])^2. \qquad (2)$$

Besides, in Fig. 4(a) for $R_A = 3$ mm the magnitude of the transmission coefficient increases for frequencies greater than 2 GHz. Spurious passbands are then expected to be out of band. In addition, W_A and θ_A have the greatest impact on the passband ripples. However, while variations of W_A affect both ripples, that is, those close to 0.5 GHz and 1 GHz, variations of θ_A only affect the ripple close to 1 GHz. Additionally, θ_A also modifies the roll-off out-of-band. Eventually, G_A has a limited impact on the magnitude of the transmission and reflection coefficients (Fig. 4(c)), and for increasing R_e, the cutoff frequency decreases (Fig. 4(e)), due to the greater distance between subsequent turns of the spirals, but less than that for R_A. Interestingly, variations on the small absolute values of W_A and G_A do not affect the response much since this mitigates the impact of production tolerances.

For a deeper insight into the working principles of the type A element, the magnitudes of surface currents at 1.0, 1.5, and 2.0 GHz are depicted in Fig. 5. Observe that at the lowest frequency, the signal propagates toward the direction of the spiral joining the inner circle; at the middle frequency, the signal propagates in both spiral arms; at the highest frequency, the signal propagates toward the direction of the spiral not joining the inner circle.

2.2. Type B Element

Element B shows etched spirals (Fig. 2(b)). The circular patch has a radius of R_B, and the etched slots have a width of W_B. S_B represents the distance between the slots in the midline between

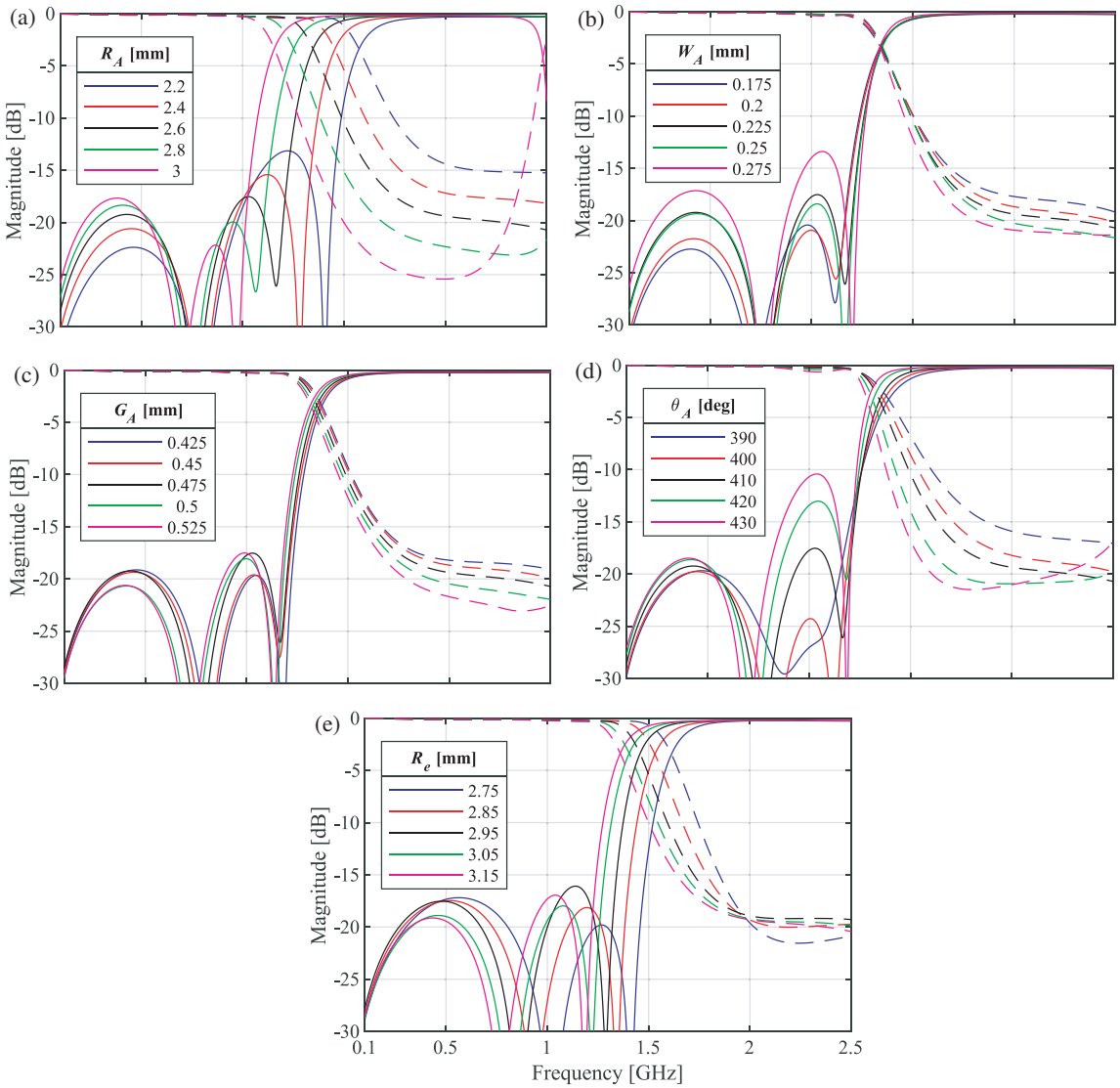

FIGURE 4. Parametric sweeps for the type A element: dashed (solid) curves for the magnitude of the transmission (reflection) coefficient.

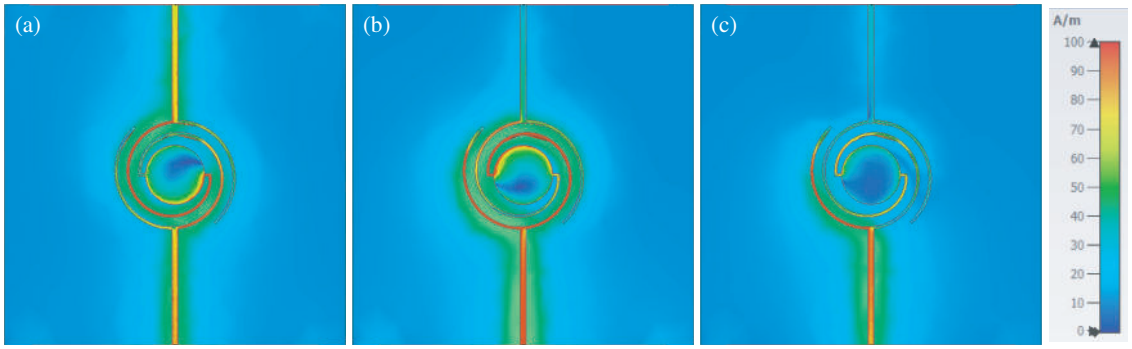

FIGURE 5. Magnitude of the surface currents for the nominal design: (a) 1.0 GHz; (b) 1.5 GHz; (c) 2.0 GHz; scale on the right.

consecutive turns, and D_B denotes the distance between the end of the spiral midline and the circumference of the circular patch. The spirals are two, symmetric with respect to the element's center. The midline of one of the spiral slots is defined as

$$\rho(\theta) = (R_B - D_B)(1 - \alpha_B \theta) \quad \theta \in [0, \theta_B] \tag{3}$$

with $\alpha_B = S_B/[\pi(R_B - D_B)]$ being a parameter that represents the wrapping speed. The type B element is defined by

five parameters: R_B, W_B, S_B, D_B, and θ_B. This element has been introduced in [6], where a thorough analysis of how these parameters impact the frequency response is presented. This analysis is analogous to the one in Fig. 4, and it is omitted for brevity since it is reported in [6].

2.3. Full Diplexer

Using a star-type (nonresonant) Y-junction [28], the two spiral resonators are joined to create the diplexer depicted in Fig. 1. The three branches of the Y-junction are evenly spaced angularly, and their lengths are L_{YA}, L_{YB}, and L_{YC}. For the type A (B) element, the distance from the end of the branch of length L_{YA} (L_{YB}) and the center of the element is L_A (L_B). For both elements, the distance between the ends of the branches and the 90°-bends have length L_Y (Fig. 1). To see the out-of-band impedances of the filtering elements as open circuits at Y-junction, the lengths L_{YA}, L_{YB}, L_A, and L_B of the microstrip traces between the filtering elements and Y-junction are optimized. Instead, the length L_Y does not affect the out-of-band impedances and should be as short as possible to pursue a compact device but not too short to avoid undesired coupling between the type B element and the microstrip line after the 90° bend. To reduce discontinuities, all microstrip bends are mitered. Eventually, the frequency ratio of the two channels is mainly controlled by the ratio of radii R_A and R_B of the two elements.

As an example, the diplexer design is considered for satellite applications at 0.87 and 2.0 GHz. As starting values for the filtering element parameters, the results in Subsection 2.1 are used for the type A element, with those in [6] for the type B element. After this first preliminary design, the device is optimized using full-wave simulations, such as [29–31]. Optimization is driven by the following goals: $|S_{11}|$ less than -10 dB in the two channels; $|S_{21}|$ ($|S_{31}|$) as close to 0 dB as possible in the lower (higher) channel to pursue a low loss device; $|S_{32}|$ less than -25 dB to attain a good isolation between the channels. The final dimensions are listed in Table 1.

TABLE 1. Dimensions of the diplexer prototype.

R_A (mm)	W_A (mm)	G_A (mm)	θ_A (deg)	R_e (mm)
2.61	0.22	0.47	408	2.95
R_B (mm)	W_B (mm)	D_B (mm)	θ_B (deg)	S_B (mm)
5.27	0.36	0.24	360	0.79
L_Y (mm)	L_{YA} (mm)	L_{YB} (mm)	L_{YC} (mm)	
38.78	4.86	5.77	10	
L_A (mm)	L_B (mm)	L (mm)	W (mm)	W_{in} (mm)
21.43	30.52	60	36	0.57

3. RESULTS

The realized diplexer is depicted in Fig. 6(a). The dimensions of the diplexer are $0.129\,\lambda \times 0.265\,\lambda \approx 0.0343\,\lambda^2$, with λ the wavelength (see Table 2). The device has been characterized using a VNA N5242A from Agilent Technologies. A three-port

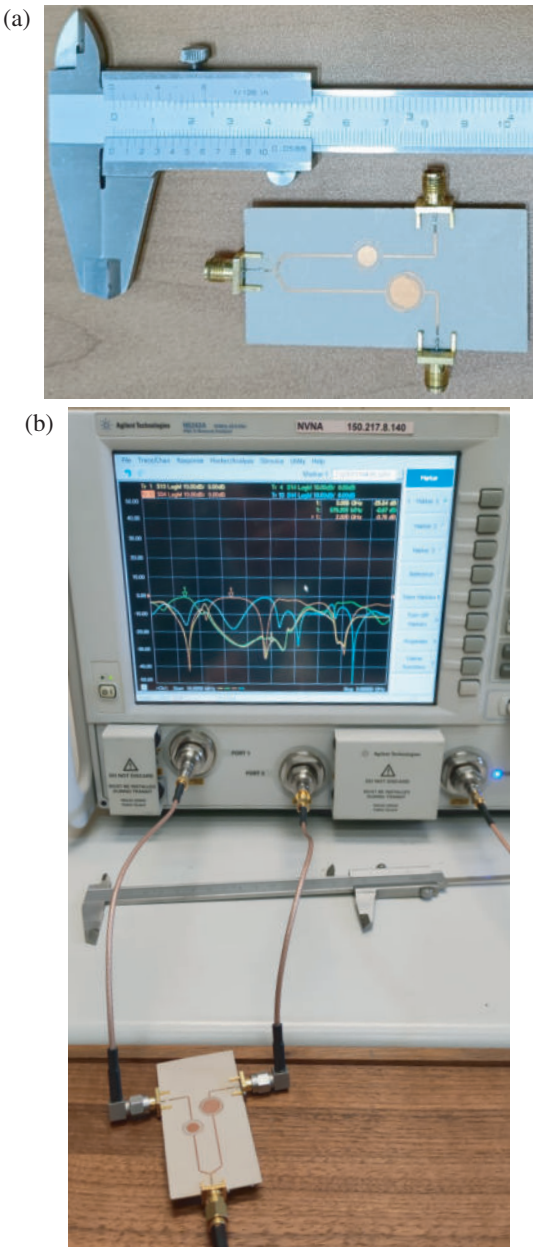

FIGURE 6. Realized prototype with SMA connectors: (a) next to a caliber; (b) during measurements.

measurement has been performed with SOLT calibration [32]. A picture of the device while performing the measurements is shown in Fig. 6(b).

The comparison between the measured and simulated results is shown in Fig. 7 in the frequency range 0.1–2.5 GHz. Overall, a satisfactory agreement is achieved between the measured and simulated data, especially in the passbands. The unavoidable discrepancies are due to the manufacturing imperfections, but they permit us to have an idea of the expected behavior. The measured performance of the device is as follows: the center frequencies are 0.87 GHz and 2.03 GHz; the -10 dB fractional bandwidths for channels A and B are 28.6 % and 27.4%, respectively; and the return loss (RL) and insertion loss (IL) at the center frequencies are given in Table 2. The measured center

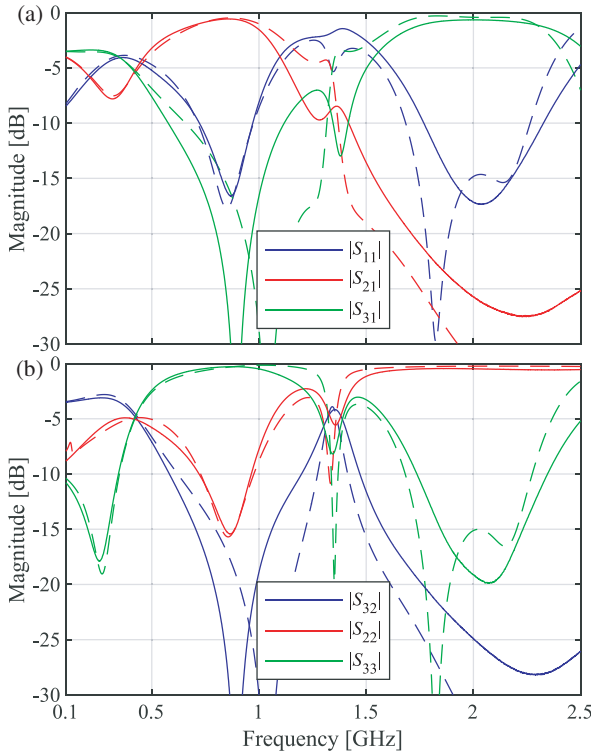

FIGURE 7. Narrow-band measured (continuous) and simulated (dashed) magnitudes of the scattering parameters: (a) $|S_{11}|$, $|S_{21}|$, and $|S_{31}|$; (b) $|S_{32}|$, $|S_{22}|$, and $|S_{33}|$. See Fig. 1 for the port numbering.

frequency for channel B is shifted from the desired frequency by 20 MHz. However, the desired signal at 2.0 GHz is within the passband of the channel. The type B element presents a transmission zero [6], which is placed in the low-pass bandwidth, thus enhancing the isolation between the channels. The isolation at the center frequencies is 32 dB and 25 dB for channels A and B, respectively. These values of isolation are comparable with those of the diplexer for satellite communications reported in [33] (27 dB), and those of the diplexers reported in [10] (24 dB) and [34] (22.7 dB and 24.4 dB for the lower and higher channels, respectively). Overall, both the simulated and measured data match the criteria characterizing a diplexer, listed at the end of the previous section, thus validating the effectiveness of the design.

In Table 2, the characteristics of the diplexer are compared with those of relevant devices in single-layer microstrip technology. The outlined diplexer has an occupied area of the same order of magnitude as the most compact diplexers [5, 35, 36], with competitive RL and IL.

For completeness, the measured wideband responses for the diplexer in the 0.1–5 GHz frequency range are plotted in Fig. 8. For both channels, spurious passbands with an IL of at least 3 dB appear for frequencies greater than 3 GHz. Depending on the specific application, these spurious passbands could be undesired; thus, they may represent a potential limitation of the proposed device. To address this possible drawback, a lowpass filter starting from 2.5 GHz may be used depending on the specific system in which the diplexer is intended to operate.

TABLE 2. Comparison between single-layer microstrip diplexers.

Ref.	$\varepsilon_{r,\text{eff}}$	f_1, f_2 [GHz]	RL [dB]	IL [dB]	area*
[5]	2.25	3.65, 5.2	$\geq 15, \geq 20$	1.35, 1.31	3.26
[35]	1.61	0.8, 0.9	21.2, 24.3	0.28, 0.29	0.86
[36]	1.60	0.78, 1.85	19, 21	0.17, 0.30	2.02
[10]	1.60	4.9, 5.9	≈ 10	2.2, 2.4	53.86
[4]	1.60	1.573, 1.924	> 20	1.08, 1.18	8.82
[3]	5.60	2.0, 3.0	22, 25	≈ 2	19.02
[34]	1.60	2.4, 2.79	27.1, 27.6	0.18, 0.39	5.63
[33]	2.70	6.7, 8.4	27.7, 31.0	0.68, 0.82	85.30
[37]	2.33	8.3, 10.0	10, 10	1.8, 1.9	7.29
This	5.5	0.87, 2.03	16.6, 17.4	0.58, 0.66	3.43

Notes. Ref. stands for reference, and f_1 and f_2 are the center frequencies of the lower and higher channels, respectively. The unit of the area* is $100\lambda^2$, with λ the wavelength $\lambda = c/(f_1\sqrt{\varepsilon_{r,\text{eff}}})$, where c is the speed of light in vacuum, $\varepsilon_{r,\text{eff}} = (\varepsilon_r + 1)/2$ the effective relative permittivity of the substrate, and ε_r the relative permittivity of the substrate.

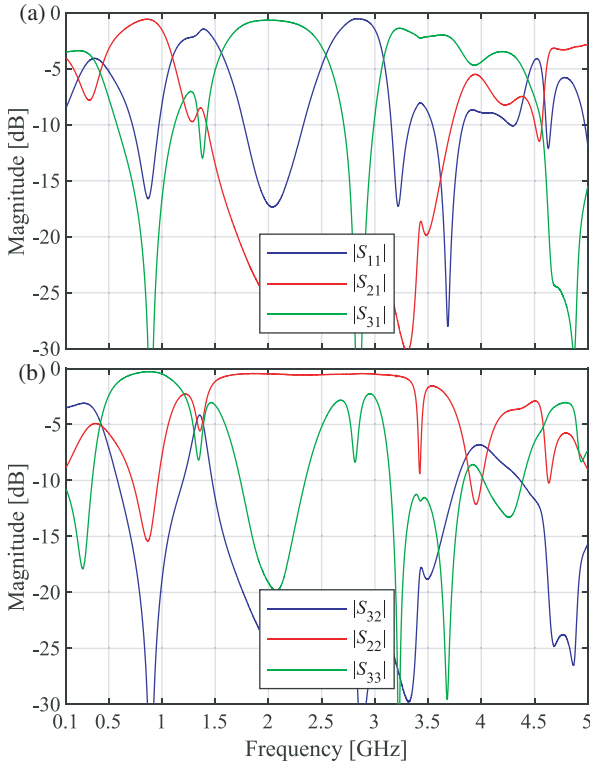

FIGURE 8. Broad-band measured magnitudes of the scattering parameters: (a) $|S_{11}|$, $|S_{21}|$, and $|S_{31}|$; (b) $|S_{32}|$, $|S_{22}|$, and $|S_{33}|$. See Fig. 1 for the port numbering.

4. CONCLUSION

A diplexer based on complementary spiral resonators is designed, manufactured, and characterized. The low-pass filtering element is novel and analyzed in the paper. The design of the diplexer is compact ($0.0343\,\lambda^2$), has low loss (IL equal to 0.58 dB for channel A and 0.66 dB for channel B), and presents suitable performance for satellite application in Europe at the

0.87 and 2.0 GHz bandwidths. The design is well supported both by simulations and measurements. Spurious out-of-band passbands occur. These might limit the usability of the diplexer depending on the requirements.

As the next steps, the authors intend to model the two spiral resonators using the coupling matrix method [28] and to perform a full-wave and circuit co-simulation technique [38] by interfacing MATLAB with HFSS [39]. Additionally, studies will be conducted to improve the compactness of the Y-junction using meandered lines.

REFERENCES

[1] Sahu, A., P. H. Aaen, and V. K. Devabhaktuni, "Advanced technologies for next-generation RF front-end modules," *International Journal of RF and Microwave Computer-Aided Engineering*, Vol. 29, No. 6, e21700, 2019.

[2] Watanabe, A. O., M. Ali, S. Y. B. Sayeed, R. R. Tummala, and M. R. Pulugurtha, "A review of 5G front-end systems package integration," *IEEE Transactions on Components, Packaging and Manufacturing Technology*, Vol. 11, No. 1, 118–133, 2020.

[3] Ogbodo, E. A., Y. Wu, P. Callaghan, and Y. Wang, "A compact diplexer with a split-ring resonator junction," *Microwave and Optical Technology Letters*, Vol. 59, No. 9, 2385–2390, 2017.

[4] García-Lampérez, A., R. Gómez-García, and M. Salazar-Palma, "Compact diplexer with edge-coupled and nonbianisotropic split-ring resonators," in *2012 IEEE/MTT-S International Microwave Symposium Digest*, 1–3, Montreal, QC, Canada, 2012.

[5] Bukuru, D., K. Song, and Xue, "Compact wide-stopband planar diplexer based on rectangular dual spiral resonator," *Microwave and Optical Technology Letters*, Vol. 57, No. 1, 174–178, 2015.

[6] Cidronali, A., G. Collodi, S. Maddio, G. Pelosi, and S. Selleri, "Quasi-elliptical band-pass filters based on compact spiral resonators for C-band applications," *Microwave and Optical Technology Letters*, Vol. 61, No. 8, 1983–1987, 2019.

[7] Cidronali, A., G. Collodi, M. Lucchesi, S. Maddio, G. Pelosi, and S. Selleri, "A multi-stage pass-band filter with ultra-compact spiral-based elements," in *2020 XXXIIIrd General Assembly and Scientific Symposium of the International Union of Radio Science*, 1–4, Rome, Italy, 2020.

[8] Giannetti, G. and S. Maddio, "Low-loss compact diplexer based on complementary spiral resonators," *Microwave and Optical Technology Letters*, Vol. 66, No. 6, e34202, 2024.

[9] Lu, K., G.-M. Wang, and H.-X. Xu, "Compact and sharp-rejection bandstop filter using uniplanar double spiral resonant cells," *Radioengineering*, Vol. 20, No. 2, 468–471, 2011.

[10] Kokkinos, T., A. P. Feresidis, and J. C. Vardaxoglou, "Analysis and application of metamaterial spiral-based transmission lines," in *2007 International workshop on Antenna Technology: Small and Smart Antennas Metamaterials and Applications*, 233–236, Cambridge, UK, 2007.

[11] Lu, K., G.-M. Wang, H.-Y. Xu, and X. Yin, "Design of compact planar diplexer based on novel spiral-based resonators," *Radioengineering*, Vol. 21, No. 1, 528–532, 2012.

[12] Bukuru, D., K. Song, and Xue, "Compact wide-stopband planar diplexer based on rectangular dual spiral resonator," *Microwave and Optical Technology Letters*, Vol. 57, No. 1, 174–178, 2015.

[13] Paredes, F., G. Zamora, F. J. Herraiz-Martinez, F. Martin, and J. Bonache, "Dual-band UHF-RFID tags based on meander-line antennas loaded with spiral resonators," *IEEE Antennas and Wireless Propagation Letters*, Vol. 10, 768–771, 2011.

[14] Lopes, B., T. Ferreira, and J. N. Matos, "Design guidelines for gap coupled spiral microstrip resonators in chipless RFID tags," *IEEE Journal of Radio Frequency Identification*, Vol. 4, No. 4, 525–531, 2020.

[15] Khan, S. R. and G. Choi, "Analysis and optimization of four-coil planar magnetically coupled printed spiral resonators," *Sensors*, Vol. 16, No. 8, 1219, 2016.

[16] Elgeziry, M., F. Costa, and S. Genovesi, "Wireless monitoring of displacement using spiral resonators," *IEEE Sensors Journal*, Vol. 21, No. 16, 17 838–17 845, 2021.

[17] ——, "Design guidelines for sensors based on spiral resonators," *Sensors*, Vol. 22, No. 5, 2071, 2022.

[18] Baena, J. D., R. Marqués, F. Medina, and J. Martel, "Artificial magnetic metamaterial design by using spiral resonators," *Physical Review B*, Vol. 69, No. 1, 014402, 2004.

[19] Brizi, D., N. Fontana, F. Costa, and A. Monorchio, "Accurate extraction of equivalent circuit parameters of spiral resonators for the design of metamaterials," *IEEE Transactions on Microwave Theory and Techniques*, Vol. 67, No. 2, 626–633, 2019.

[20] Lee, Y.-T., J.-S. Lim, C.-S. Kim, D. Ahn, and S. Nam, "A compact-size microstrip spiral resonator and its application to microwave oscillator," *IEEE Microwave and Wireless Components Letters*, Vol. 12, No. 10, 375–377, 2002.

[21] Electronic Communications Committee, "The European table of frequency allocations and applications in the frequency range 8.3 kHz to 3000 GHz (ECA table)," in *Proceedings of European Conference of Postal and Telecommunications Administrations*, Electronic Communications Committee, Copenhagen, Denmark, 2013.

[22] Baena, J. D., J. Bonache, F. Martin, R. M. Sillero, F. Falcone, T. Lopetegi, M. A. G. Laso, J. Garcia-Garcia, I. Gil, M. F. Portillo, and M. Sorolla, "Equivalent-circuit models for split-ring resonators and complementary split-ring resonators coupled to planar transmission lines," *IEEE Transactions on Microwave Theory and Techniques*, Vol. 53, No. 4, 1451–1461, 2005.

[23] Garcia-Garcia, J., F. Martin, F. Falcone, J. Bonache, J. D. Baena, I. Gil, E. Amat, T. Lopetegi, M. A. G. Laso, J. A. M. Iturmendi, M. Sorolla, and R. Marques, "Microwave filters with improved stopband based on sub-wavelength resonators," *IEEE Transactions on Microwave Theory and Techniques*, Vol. 53, No. 6, 1997–2006, 2005.

[24] Collin, R. E., *Foundations for Microwave Engineering*, John Wiley & Sons, 2007.

[25] Dassault Systèmes, "CST Studio Suite," [Online]. Available: https:// www.3ds.com/products-services/simulia/products/cst-studio-suite/, 2023.

[26] Gentili, G. G., G. Giannetti, M. Khosronejad, G. Pelosi, and S. Selleri, "Modes computation in arbitrarily shaped waveguides by a transformation optics approach," *International Journal of RF and Microwave Computer-Aided Engineering*, Vol. 31, No. 1, e22480, 2021.

[27] Gentili, G. G., G. Giannetti, G. Pelosi, and S. Selleri, "Considerations on boundary conditions in transformation optics for complete field computation in generic waveguides," *Microwave and Optical Technology Letters*, Vol. 65, No. 1, 373–380, 2023.

[28] Cameron, R. J., C. M. Kudsia, and R. R. Mansour, *Microwave Filters for Communication Systems: Fundamentals, Design, and Applications*, John Wiley & Sons, 2018.

[29] Pelosi, G., S. Selleri, and R. Taddei, "A novel multiobjective Taguchi's optimization technique for multibeam array synthesis," *Microwave and Optical Technology Letters*, Vol. 55, No. 8, 1836–1840, 2013.

[30] Maddio, S., G. Pelosi, M. Righini, and S. Selleri, "A multi-objective invasive weed optimization for broad band sequential rotation networks," in *2018 IEEE International Symposium on Antennas and Propagation & USNC/URSI National Radio Science Meeting*, 955–956, IEEE, 2018.

[31] Sengupta, S., S. Basak, and R. A. Peters, "Particle swarm optimization: A survey of historical and recent developments with hybridization perspectives," *Machine Learning and Knowledge Extraction*, Vol. 1, No. 1, 157–191, 2018.

[32] Rumiantsev, A. and N. Ridler, "Vna calibration," *IEEE Microwave Magazine*, Vol. 9, No. 3, 86–99, 2008.

[33] Upadhyaya, T., J. Pabari, V. Sheel, A. Desai, R. Patel, and S. Jitarwal, "Compact and high isolation microstrip diplexer for future radio science planetary applications," *AEU — International Journal of Electronics and Communications*, Vol. 127, 153497, 2020.

[34] Rezaei, A., L. Noori, and H. Mohammadi, "Design of a novel compact microstrip diplexer with low insertion loss," *Microwave and Optical Technology Letters*, Vol. 59, No. 7, 1672–1676, 2017.

[35] Rezaei, A. and L. Noori, "Novel compact microstrip diplexer for GSM applications," *International Journal of Microwave and Wireless Technologies*, Vol. 10, No. 3, 313–317, 2018.

[36] Rezaei, A., S. I. Yahya, and M. H. Jamaluddin, "A novel microstrip diplexer with compact size and high isolation for GSM applications," *AEU — International Journal of Electronics and Communications*, Vol. 114, 153018, 2020.

[37] Dembele, S. N., J. Bao, T. Zhang, and D. Bukuru, "Compact microstrip diplexer based on dual closed loop stepped impedance resonator," *Progress In Electromagnetics Research C*, Vol. 89, 233–241, 2019.

[38] Shin, S. and S. Kanamaluru, "Diplexer design using EM and circuit simulation techniques," *IEEE Microwave Magazine*, Vol. 8, No. 2, 77–82, 2007.

[39] Giannetti, G., "Improved and easy-to-implement HFSS-MATLAB interface without VBA scripts: An insightful application to the numerical design of patch antennas," *Applied Computational Electromagnetics Society Journal*, Vol. 38, 377–381, 2023.